engineering proceedings

MDPI

Proceeding Paper

Study of Lightweight Frames for Electrically Power-Assisted Cycles †

Emanuele Vincenzo Arcieri * and Sergio Baragetti

Department of Management, Information and Production Engineering, University of Bergamo, Viale Marconi 5, 24044 Dalmine, BG, Italy; sergio.baragetti@unibg.it

* Correspondence: emanuelevincenzo.arcieri@unibg.it

† Presented at the 54th Conference of the Italian Scientific Society of Mechanical Engineering Design (AIAS 2025), Florence, Italy, 3–6 September 2025.

Abstract

This study investigates the structural performance of a lightweight frame for electrically power-assisted cycles (EPACs) subjected to a variable loading at the front axle, in accordance with the reference standard. A finite element model was developed to evaluate the stress distribution in the frame and was validated through experimental testing using uniaxial strain gauges. Finite element and experimental stress values showed good agreement, confirming the reliability of the model in predicting the global structural response. Experimental results and fatigue considerations based on finite element results indicate that the frame strength is largely verified under the prescribed loading condition. The validated model therefore provides a robust tool for supporting the design and optimization of EPAC frames.

Keywords: EPAC; lightweight; structural behavior; FEM; experimental testing

1. Introduction

Electrically power-assisted cycles (EPACs) represent a sustainable mobility solution which contributes to reduced urban emissions and promotes active transportation. Their diffusion has grown significantly in recent years, due to technological advancements and increasing environmental sensitivity. EPACs offer a feasible alternative to conventional vehicles for short- and medium-range commuting, contributing to the decarbonization of transport systems. By assisting pedaling, EPACs significantly lessen human effort and make cycling more accessible to a broader range of users. Moreover, they can help reduce urban traffic congestion by replacing car trips with smaller vehicles and more flexible modes of transport [1,2].

The frame of an EPAC is the principal load-bearing structure and must have sufficient stiffness to resist bending and torsional loads. For this reason, particular attention must be paid to its design both in terms of material selection and geometry. The adoption of lightweight alloys or composite materials [3–6] enables for instance the development of frames with superior strength-to-weight ratios. The geometry of the frame significantly influences dynamic behavior, rider ergonomics and aerodynamic efficiency. To ensure rider comfort and structural durability, the frame must also attenuate road-induced vibrations, even if controlled vibration reduction systems may be mounted [7]. Concurrently, integrating electrical components, such as the motor, battery pack and cabling systems within the frame architecture of EPACs introduces additional mass and alters internal force

Academic Editors: Nicola Bonora, Umberto Galietti, Luigi Bruno, Davide Castagnetti, Cristiana Del Prete, Mario Guagliano and Vigilio Fontanari

Published: 1 April 2026

distribution during pedaling. This implies the necessity of designing cable channels and mounting interfaces that do not produce stress concentrations or compromise overall frame stiffness [8]. Nowadays, foldable and portable architectures are also emerging so that users can easily store or transport EPACs in compact environments, such as trains, buses and elevators [9].

Finite element analysis can guide the design process of e-bike frames. In [3], unidirectional epoxy carbon composite prepreg and epoxy carbon woven prepreg were numerically tested as candidate materials for mountain e-bike frames. Lee et al. [8] proposed a method to improve frame fatigue strength based on finite element analysis. Xiao et al. [10] used the finite element method to optimize material distribution in the frame and achieve enhanced stiffness. Similarly, Cahyono et al. [11] conducted finite element analysis to improve the structural performance of a three-wheel electric bicycle frame.

The scope of this work is to assess the structural performance of an aluminum EPAC frame subjected to one of the loading cases prescribed by the reference standard. A finite element model was created to predict the stress distribution in the frame and was validated through experimental testing. Simplified fatigue considerations based on the finite element results were used to obtain a rough evaluation of the fatigue strength of the frame, which successfully passed the experimental test. The validated model therefore provides a reliable tool for supporting the design and optimization of lightweight EPAC frames.

2. Finite Element Analysis

The study was conducted on the aluminum 6061-T6 EPAC frame shown in Figure 1. In such frames, the integration of the motor unit, battery pack and associated mounting interfaces requires a redistribution of material and an increase in local wall thicknesses compared with traditional frames, particularly in the down tube, seat tube and motor housing region, which lead to a slightly different architecture.

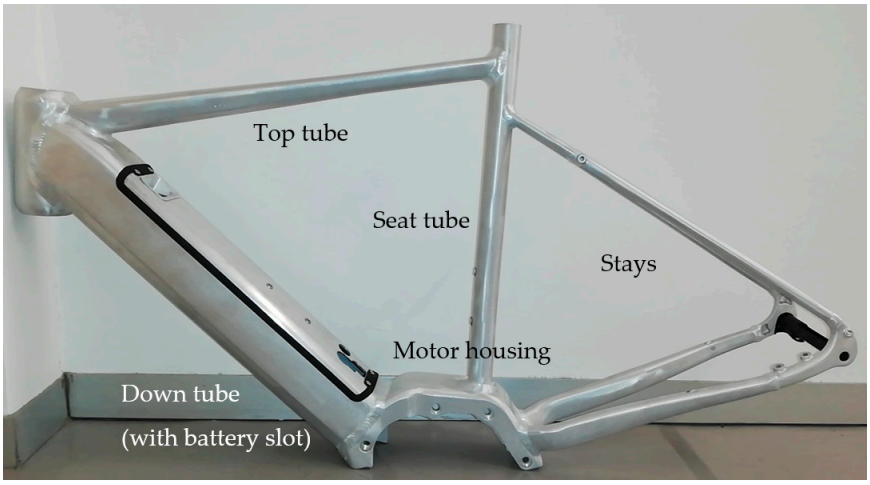

Figure 1. Aluminum EPAC frame.

The reference safety and technical standard for EPACs is UNI EN ISO 15194:2023 [12] and one of the prescribed tests is the fatigue test with horizontal forces, whose scheme is shown in Figure 2. According to the standard, fatigue testing must be performed with a loading frequency not exceeding 10 Hz and the applied force must range from 600 N in tension to 600 N in compression. The standard prescribes a fatigue life of 100,000 loading cycles. The use of the original fork is not mandatory, provided that the used dummy fork has the intended fork length and an adequate stiffness and is correctly installed in the head tube.

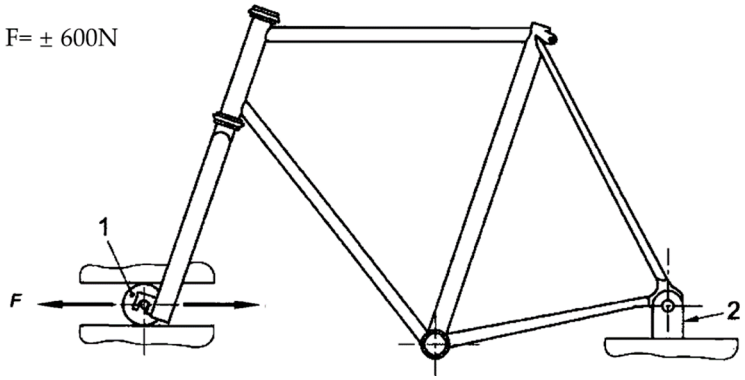

Figure 2. Fatigue test with horizontal forces, with 1 indicating the free-running guided roller and 2 the rigid, pivoted mounting for rear axle attachment point [12].

The frame was modeled in Abaqus 2022 using two-dimensional shell elements (S4R and S3R for mesh transitions), since it is composed of thin-walled tubular components. The external surfaces of individual parts were selected as reference geometry and the wall thicknesses were modelled inward. Uniform thicknesses were assigned to the frame components: the seat tube and the top tube have a thickness of 2.3 mm; the stays of 2 mm; the down tube of 4 mm; the head tube of 3 mm; the engine casing of 6 mm. The joint element connecting the two stays, where the rear pin is mounted, was modeled using C3D10 three-dimensional elements due to its large thickness. The support structures designed to conduct the experimental test and the dummy fork were modelled with C3D8R three-dimensional elements. The front and rear pins for the mounting of the frame on the testing machine were modelled with B31 beam finite elements. The resulting model is shown in Figure 3 and consists of 23 B31 elements, 70 S3R elements, 201,734 S4R elements, 14,456 C3D8R elements and 7437 C3D10 elements, as determined through a mesh-convergence study. Mesh details in the proximity of the head tube and in the proximity of the joint element connecting the stays are shown in Figures 3a and 3b, respectively. Actually, only half of the assembly containing the frame and supports was modeled, due to the presence of a symmetry plane (Figure 3c). Fillets and chamfers considered irrelevant to structural calculation and welds between frame elements were intentionally not modelled to optimize computational efficiency.

The material properties assigned to the aluminum bicycle frame are a Young's modulus of 69,000 MPa and a Poisson's ratio of 0.34. Even the properties of the steel used in the support systems were defined, with a Young's modulus of 210,000 MPa and a Poisson's ratio of 0.3. Both materials were assumed to be homogeneous, isotropic and linear elastic.

Two load steps, which can be named "tension" and "compression", were defined to simulate the extreme conditions of the alternating symmetric fatigue loading prescribed by the standard. Geometric nonlinearity was included in the analysis to take into consideration large-displacement effects on the structural response of the frame. Kinematic constraints were used to model the connections between the supports and the frame components. Couplings were used to rigidly connect the stays to the dropout. Additional couplings were adopted to create rigid connections between the rear pin end node and the corresponding hole of the dropout and between the front pin and its support (the latter is shown in Figure 3d). Two couplings were used to simulate bearings between the head tube and the fork stem, locking relative rotation between the connected regions. Tie constraints were applied to simulate rigid connections between the stem and plate surfaces and between the upper surface of the pin support and the lower surface of the plate.

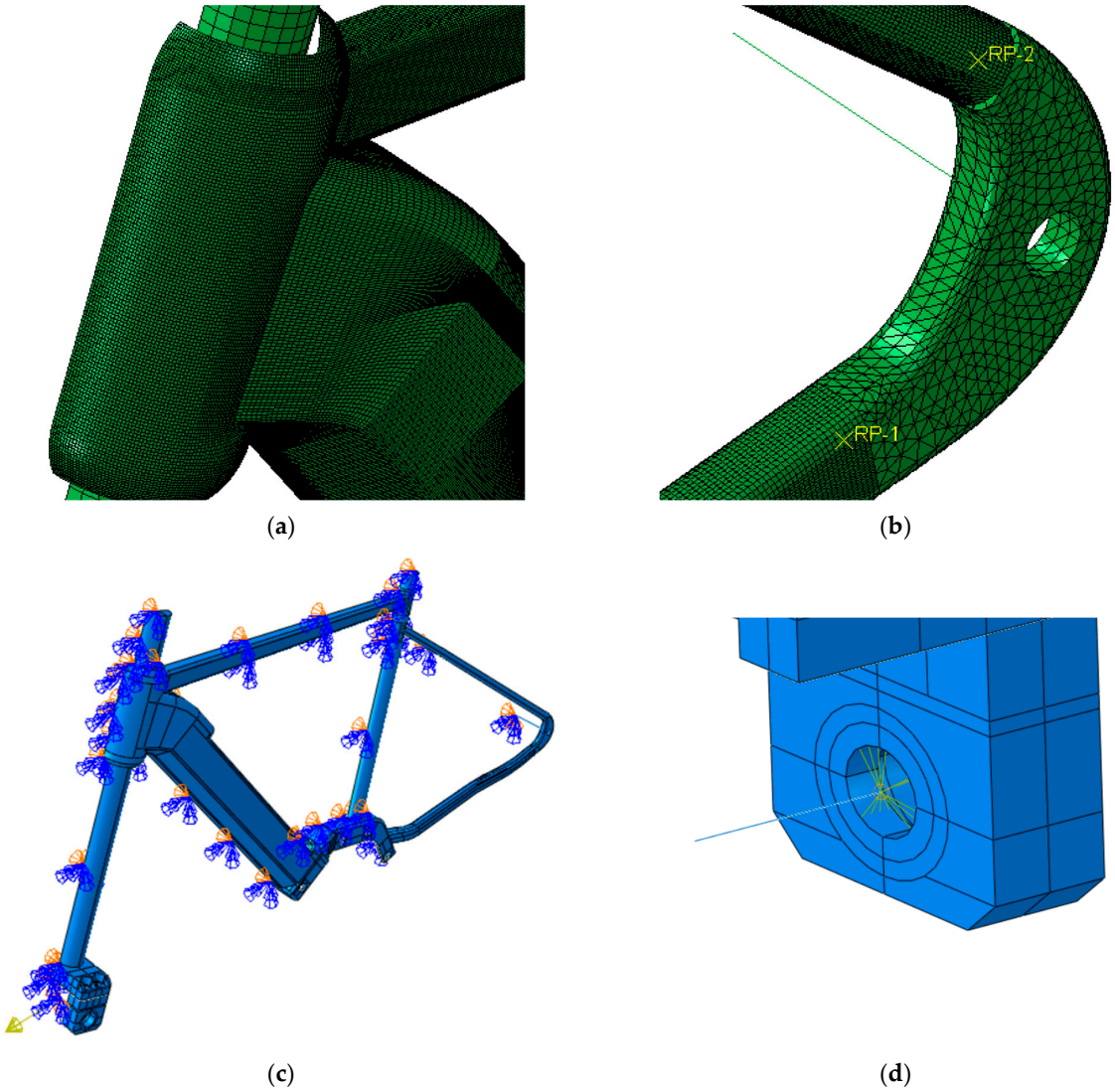

Figure 3. Finite element model of the EPAC assembly: (**a**) mesh detail in the proximity of the head tube (2D finite elements used for the frame and 3D elements for the fork); (**b**) mesh detail in the proximity of the joint element connecting the stays (stays modelled with 2D elements, dropout with 3D elements and rear pin with 1D elements); (**c**) schematic of the model, with the loading and boundary conditions for the case with tension force; (**d**) schematic of the connection between the front pin and the fork support (the geometry partitions created to improve the mesh quality are visible; the fork support is modelled with 3D elements, the pin is modelled as a 1D structure).

A horizontal concentrated force was imposed at the mid-node of the front pin. Since only half of the frame was modeled, a force of 300 N was applied forward in the "tension" load step, while a force of 300 N was applied backward in the "compression" load step. Symmetry conditions were applied. Further boundary conditions were defined according to the reference standard (see again Figure 3c).

Table 1 reports the maximum Von Mises stresses reached in the different parts of the analyzed EPAC frame. The stress distribution under maximum compressive loading is shown in Figure 4 as a reference. Table 2 reports the obtained values of maximum displacement (in magnitude) in the frame and in the whole simulated assembly. The highest displacement in the frame is observed in the down tube region near the head tube. In the complete assembly, the maximum displacement occurs near the point of force application. The stress and displacement values under tension and compression are substantially equivalent.

https://doi.org/10.3390/engproc2026131027

Table 1. Von Mises stresses according to finite element results.

Location	Load Step	Von Mises Stress (MPa)
head tube, lower bearing mount	compression tension	29.5 29.6
head tube, lower junction with down tube	compression tension	21.5 21.5
down tube, battery housing notch	compression tension	47.5 47.3
top tube, lower junction with head tube	compression tension	17.8 17.7
seat tube, rear junction with motor housing	compression tension	14.7 14.6
motor housing, rear junction with seat tube	compression tension	14.5 14.4
stays, curvature near motor housing	compression tension	15.3 15.2
stays, junction with seat tube	compression tension	5.9 5.8
dropout, hole for rear axle	compression tension	6.9 6.8
cross member, junction with seatstays	compression tension	1.7 1.7

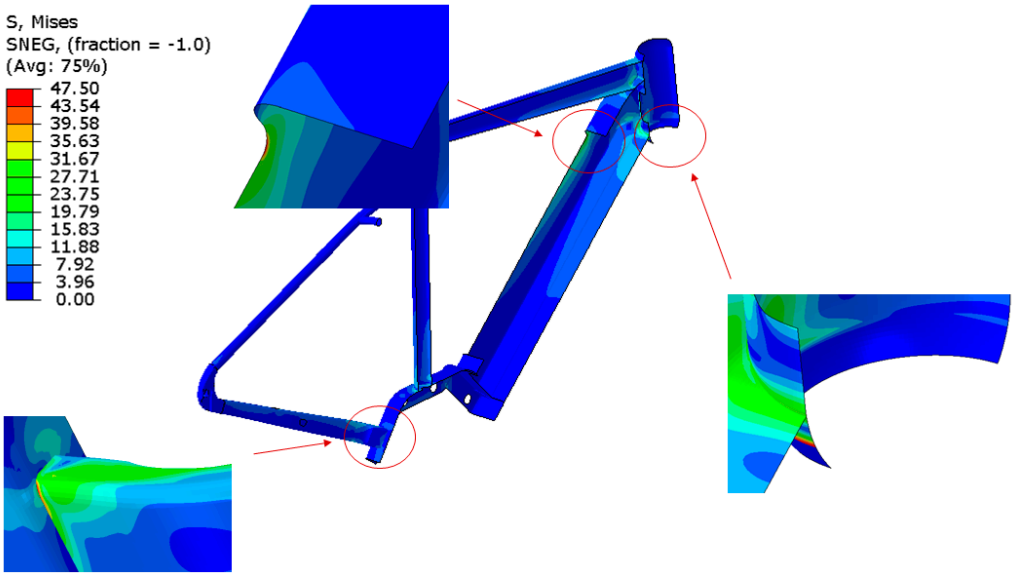

Figure 4. Von Mises stresses under compression loading (MPa).

Table 2. Maximum displacement in the frame and in the whole assembly.

Configuration	Load Step	Displacement (mm)
without support components	compression tension	0.6 0.6
with support components	compression tension	1.4 1.4

https://doi.org/10.3390/engproc2026131027

3. Experimental Test and Validation of the Finite Element Model

The experimental fatigue test was performed in accordance with the reference standard. To validate the finite element model, uniaxial strain gauges were placed on the frame in the positions illustrated in Figure 5. The model was developed using shell elements for the EPAC frame and is therefore expected to provide a reliable representation of the membrane and bending stresses in the thin-walled tubes. However, it may not fully capture the local stress concentrations that may arise at tube connections and geometric discontinuities. It should also be noted that welds were not modelled. It is for this reason that the strain gauges were mounted far from the areas where the different parts of the frame intersect.

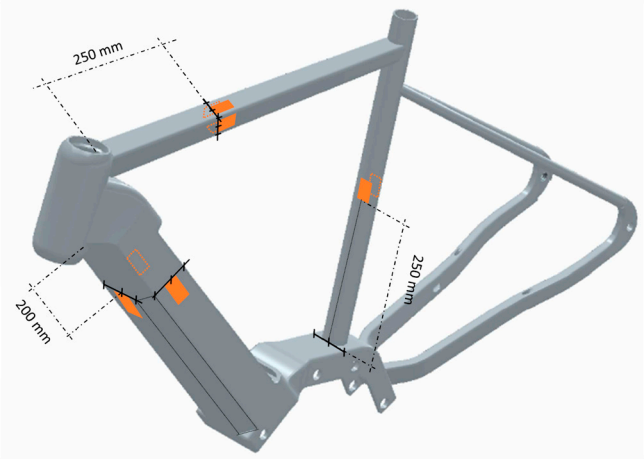

Figure 5. Position of the strain gauges on the EPAC frame.

Figure 6 shows the frame mounted on the testing machine located in the Research Group's laboratory at the School of Engineering of the University of Bergamo, in Dalmine (BG).

Figure 6. Frame mounted on the testing machine.

Figure 7 presents the time evolution of axial stresses obtained with the strain gauges in five reference cycles, selected from the 100,000 cycles applied during the fatigue test. The peak stress values observed during the entire test remained substantially constant, indicating the absence of material yielding or failure.

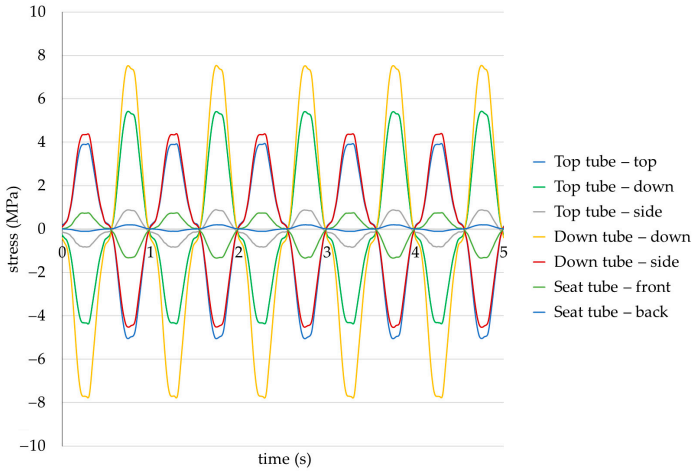

Figure 7. Axial stresses in five reference cycles.

To assess the accuracy of the finite element model, stress values measured with the strain gauges were averaged over time for both the maximum and minimum force conditions. These values were then compared with the results obtained from the finite element simulation, as shown in Table 3. Percentage discrepancies are not included, as stress magnitudes in some locations are very low and the quantitative comparison of the results could lead to high relative errors which are misleading. The absolute differences between experimental and numerical stress levels remain below 2 MPa in all cases. This indicates that the finite element model provides a sufficiently accurate representation of the experimental behavior and can therefore be considered validated.

Table 3. Comparison of the experimental and finite element results.

		Top Tube—Top	Top Tube—Down	Top Tube—Side	Down Tube—Down	Down Tube—Side	Seat Tube—Front	Seat Tube—Back
compression	experimental (MPa)	3.7	−4.1	−0.7	−7.6	4.3	0.7	−0.1
	finite element model (MPa)	3.7	−5.0	−0.1	−6.0	3.4	2.4	−1.3
tension	experimental (MPa)	−5.0	5.4	1.0	7.3	−4.4	−1.3	0.3
	finite element model (MPa)	−3.7	5.0	0.1	6.1	−3.3	−2.4	1.1

A detailed visual inspection was carried out on all critical regions of the frame at the end of the fatigue test, with particular attention to welded joints, geometric discontinuities and areas subjected to the highest stress levels. No cracks or fractures were observed in the frame, indicating that the structural strength was adequate for the prescribed loading condition. An in-depth experimental assessment of the possible cumulative damage at the end of the fatigue test was not performed. However, a rough estimation could be made by comparing the number of executed cycles with the fatigue life expected under an alternating stress equal to the maximum von Mises stress obtained with the finite

element calculation, i.e., 47.5 MPa, following the Miner's rule. As a first approximation, an admissible stress equal to the ultimate tensile stress of the material, that is 290 MPa for 6061-T6 aluminum alloy [13], can be considered to correspond to a fatigue life of 1000 cycles under fully reverse loading, and an admissible stress equal to 0.33 times the ultimate tensile strength (i.e., 96 MPa) can be assumed at 2,000,000 cycles. By cautiously introducing a dimensional factor equal to 0.7 and a surface factor of 0.8, an admissible stress of approximately 54 MPa is obtained for 2,000,000 cycles. The stress concentration factor does not need to be explicitly considered in this analysis on fatigue strength, since the finite element model already accounts for geometric stress raisers where they are modelled. As can be seen, the maximum stress resulting from the finite element analysis is approximately equal to the estimated admissible stress at 2,000,000 cycles. This implies that the damage accumulated by the frame in the 100,000 cycles of the test is roughly 1/20. The same conclusions can be drawn by considering the maximum principal stress in magnitude among the simulated tension and compression loading cases, which is 47.9 MPa and thus very close to the maximum von Mises stress. It should also be noted that the finite element results include the static stress concentration factor, which is equal to or higher than the fatigue stress concentration factor, as the latter is reduced by notch sensitivity effects. Even though this discussion involves several assumptions and simplifications, it provides a reasonable indication that the fatigue strength of the frame is largely satisfied under the tested loading condition. This result can be attributed to different factors. First of all, in real-world applications, the EPAC is equipped with the battery and the motor, which alters the load distribution and requires increased thickness in some regions of the frame. Secondly, the frame must also provide an adequate stiffness, which influences the behavior of the EPAC and the rider comfort. Finally, the reference standard prescribes other tests, which are beyond the scope of the present work. However, the created finite element model can be used to identify the most stressed areas and offer insights for optimizing the frame geometry.

4. Conclusions

The stress distribution in an aluminum EPAC bicycle frame subjected to the extreme conditions of a fatigue loading case prescribed by the reference standard was assessed through finite element analysis. The comparison between experimental measurements and finite element predictions demonstrated good agreement, with discrepancies remaining quantitatively negligible. The frame successfully passed the experimental fatigue test, and simplified considerations based on the finite element results further support the adequacy of its structural performance under the prescribed loading condition. The consistency between the numerical and experimental results demonstrates the reliability of the numerical model, which is able to provide the global stress state in the frame and thereby allows the identification of potential critical regions or improvement actions to enhance the strength-to-mass ratio.

Author Contributions: Conceptualization, E.V.A. and S.B.; methodology, E.V.A. and S.B.; software, E.V.A. and S.B.; validation, E.V.A. and S.B.; formal analysis, E.V.A. and S.B.; investigation, E.V.A. and S.B.; resources, E.V.A. and S.B.; data curation, E.V.A. and S.B.; writing—original draft preparation, E.V.A.; writing—review and editing, S.B.; visualization, E.V.A. and S.B.; supervision, E.V.A. and S.B. All authors have read and agreed to the published version of the manuscript.

Funding: The activity was conducted within the project National Center for Sustainable Mobility—MOST, funded by the European Union—Next Generation EU, PNRR—M4C2 INV. 1.4 (CN00000023–CUP F13C22000690001).

Institutional Review Board Statement: Not applicable.

Informed Consent Statement: Not applicable.

Data Availability Statement: Data are available upon request.

Acknowledgments: The authors wish to thank Michele Giudici, Luca Flaminio Sorti and Francesco Foieni for their help.

Conflicts of Interest: The authors declare no conflicts of interest.

References

1. Stilo, L.; Segura-Velandia, D.; Lugo, H.; Conway, P.P.; West, A.A. Electric bicycles, next generation low carbon transport systems: A survey. *Transp. Res. Interdiscip. Perspect.* **2021**, *10*, 100347. [CrossRef]
2. Salmeron-Manzano, M.; Manzano-Agugliaro, F. The electric bicycle: Worldwide research trends. *Energies* **2018**, *11*, 1894. [CrossRef]
3. Yasin, H.I.; Darsin, M.; Jatisukamto, G. Finite element analysis on e-bike frame model with composite material variations. *AIP Conf. Proc.* **2023**, *2482*, 120001. [CrossRef]
4. Iskandar, R.; Sawitri, D.; Hantoro, R.; Zulkifli, I.; Pratama, Y. Analysis of static mechanical properties of electric bike frames using finite element analysis (FEA). *AIP Conf. Proc.* **2021**, *2384*, 070004. [CrossRef]
5. Niranjana, S.J.; Shivakumar, S.; Raghavendra, S.; Ravikumar, H.C. Design and Stress Analysis of the Frame for an Electric Bike. In *Proceedings of the Second Congress on Control, Robotics and Mechatronics*; Jha, P.K., Jamwal, P., Tripathi, B., Garg, D., Sharma, H., Eds.; Springer: Singapore, 2024. [CrossRef]
6. Atmika, I.K.A.; Subagia, I.D.G.A.; Surata, I.W.; Sutantra, I.N.; Suriadi, I.G.A.K. Study of Mechanical Properties of Hemp Fiber Composites for Electric Bicycle Frames. *Mater. Sci. Forum* **2020**, *1000*, 167–172. [CrossRef]
7. Meng, C.-L.; Bui, V.-T.; Dow, C.-R.; Chang, S.-M.; Lu, Y.-E. A Road-Adaptive Vibration Reduction System with Fuzzy PI Control Approach for Electric Bicycles. *World Electr. Veh. J.* **2025**, *16*, 276. [CrossRef]
8. Lee, S.-Y.; Jiang, C.-P.; Lee, C.-K.; Huang, W.-H.; Cheng, Y.-C. Optimization of design and fatigue simulations for an electric assisted bicycle frame using uniform design and grey relational analysis. *J. Strain Anal. Eng. Des.* **2023**, *58*, 3–16. [CrossRef]
9. Mia, M.F.; Rahman, M.M.; Islam, M.A.; Sifat, F.H.; Ahamed, T.; Sharuf, M. Design and Construction of Portable Electric Bicycle. In Proceedings of the 2025 International Conference on Cognitive Computing in Engineering, Communications, Sciences and Biomedical Health Informatics, Uttar Pradesh, India, 16–18 January 2025.
10. Xiao, D.; Liu, X.; Du, W.; Wang, J.; He, T. Application of topology optimization to design an electric bicycle main frame. *Struct. Multidiscip. Optim.* **2012**, *46*, 913–929. [CrossRef]
11. Cahyono, S.I.; Anwar, M.; Diharjo, K.; Triyono, T.; Hapid, A.; Kaleg, S. Finite element analysis of electric bicycle frame geometries. *AIP Conf. Proc.* **2017**, *1788*, 030084. [CrossRef]
12. *UNI EN ISO 15194:2023*; Cycles—Electrically Power Assisted Cycles—EPAC Bicycles. Ente Nazionale Italiano di Unificazione (UNI): Milan, Italy, 2023. Available online: https://conto.uni.com/en/uni-en-15194-2023 (accessed on 19 April 2024).
13. MatWeb. Available online: www.matweb.com (accessed on 25 January 2026).